J. Plasma Phys. (2023), *vol*. 89, 905890102
Published by Cambridge University Press.

doi:10.1017/S0022377822001027

Sheath formation time for spherical Langmuir probes

Kai Morgan Kjølerbakken [1,2], **Wojciech J. Miloch** [1] **and Ketil Røed** [1]

[1]Department of Physics, University of Oslo, Oslo 0316, Norway

[2]Norwegian Institute for Air Research, Kjeller 2007, Norway

(Received 5 December 2021; revised 26 September 2022; accepted 28 September 2022)

The formation time of the surrounding sheath of Langmuir probes in an ionospheric plasma has been studied to better understand the constraints this puts on the sampling frequency of a probe. A fully kinetic three-dimensional particle-in-cell model is used to simulate the temporal effects in the electron saturation region as the sheath forms. The stability of the probe current and the stability of the ion and electron density in the vicinity of the probe have been used to evaluate when the sheath was formed. Simulated results were compared with theoretical models and are in good agreement with the theoretical results. This shows that theoretical models can be used as guidance to estimate the formation time and to determine the sampling rate for a swept bias Langmuir system. Our results also show that the formation time is less affected by the plasma temperature and bias voltage as we move into the thick sheath regime, and will instead be determined by the plasma density. The presented results also show that applying a step function to the probe could be used to characterise ions species composition, or to estimate the ion density.

Key words: electric discharges, astrophysical plasmas

1. Introduction

Time-resolved measurements of plasma fluctuations in the ionosphere are essential to understand instabilities and turbulence in the polar ionosphere and the energy transfer, transport and coupling between different scales in the near Earth space. They have also practical importance as they influence radio propagation to distant places and satellite communications (Basu, MacKenzie & Basu 1988) and represent the largest source of errors in global navigation satellite systems (Moen *et al.* 2013; Jin, Moen & Miloch 2014; Follestad *et al.* 2020). Langmuir probes are inexpensive and widely adapted instruments within space applications as well in laboratory experiments to e3characterisation of plasma quantities. However, to measure fluctuations in plasma, the temporal resolution of the system is critical. Temporal limitations for a swept Langmuir probe are related to the time required for the charged particles to form the sheath, and the time required to traverse this sheath to give a stable readout of the collected current from the probe. The sheath

formation time sets limits on the sweeping frequency of the Langmuir system, which subsequently sets the temporal limitation of the system.

Electric sheaths are present in any plasma where boundaries occur. The boundary can be confined to a finite volume or to the surfaces of an object, like a spacecraft, dust or an instrument immersed into the plasma. The plasma sheath is one of the oldest problems addressed in plasma physics, and it is still not fully understood. The basic theory of the sheath transition was first revealed by Mott-Smith & Langmuir (1926) and was further extended in the work of Bohm by a clear interpretation of the sheath, which was later introduced by Boyd (1951) as the Bohm criterion. A full self-consistent kinetic analysis of the collisionless presheath was developed by Riemann (1991). Most theories are based on the interaction between electric forces and charged particles. However, it has also been shown that in low temperature plasma (where the ion temperature excels the electron temerature, $T_e \ll T_i$) an electron pressure gradient accelerates the electrons in the sheath region to a velocity that exceeds the thermal velocity, and the sheath formation can be far more complicated than previously assumed (Scheiner *et al.* 2015).

In this study, we seek to understand the temporal properties of the sheath related to plasma parameters similar to those in the ionosphere. However, some assumptions have been made to simplify the study: we assume the enclosing plasma to be quasi-neutral, and we assume the plasma to be collision free, also in the sheath regions. This simplification will presumably affect our result. Nevertheless, the results should give a reasonable indication of the time scale and should be suitable as a guideline when operating Langmuir probes.

The paper is arranged as follows: § 2 introduces the sheath theory. In § 3, the theory behind temporal effects is presented, while theory related to the probe current is presented in § 4. In § 5, the numerical method is briefly described together with the details for the numerical set-up. In § 6, results for selected cases are presented. Finally, § 7 summarises the key findings with concluding remarks.

2. Shielding sheaths

The sheath will couple the probe potential to the quasi-neutral plasma, where the difference in charge density between electrons and positive ions equals out the probe potential towards the sheath edge. For a charged probe or when a bias voltage is applied to the probe, equally charged particles are repelled and particles with opposite charge are attracted. This imbalance in charge density results in a sheath in the vicinity of the probe, where the current of attracted particles will be limited. Outside this sheath, there will be a presheath where quasi-neutrality is preserved. However, particles in the presheath will be accelerated towards the probe due to pressure gradients. The common definition of the sheath edge is the location where charge neutrality breaks down. Charged particles need to enter the sheath edge with a velocity greater than the Bohm velocity (Riemann 1991; Scheiner *et al.* 2015). The Bohm speed is derived from the particle density n, particle velocity v, particle temperature T and particle mass m, for respectively the ions i and the electrons e by the following equations: conservation of charge flux

$$n_i v_i = n_{i0} v_{i0}, \tag{2.1}$$

conservation of energy,

$$\tfrac{1}{2} m_i v_i^2 + \phi Z e = \tfrac{1}{2} m_i v_{i0}^2, \tag{2.2}$$

the Boltzmann relation,

$$n_e(x) = n_{e0} \exp\left(\frac{e\phi}{k_B T_e}\right), \tag{2.3}$$

https://doi.org/10.1017/S0022377822001027 Published online by Cambridge University Press

and Poisson's equation,

$$\frac{\mathrm{d}^2\phi}{\mathrm{d}x^2} = -\frac{e}{\epsilon_0}(n_i - n_e), \tag{2.4}$$

where n_{i0} and v_{i0} are the ion density and velocity at the sheath edge, k_B is the Boltzmann constant, ϕ is the potential and Z is the ion charge in units of the elementary charge e. The Bohm criterion combine these equations at the sheath edge where $|e\phi| \ll k_B T_e$, making the assumption that the ion speed is much larger than the ion thermal speed, $v_i \gg v_{thi}$, and that the potential is zero in the plasma away from the sheath

$$k_B T_e \leq m_i v_o^2. \tag{2.5}$$

At the edge of the sheath this can be rearranged to define the Bohm speed

$$v_B = \left(\frac{k_B T_e}{m_i}\right)^{1/2}. \tag{2.6}$$

If the sheath is dominated by ions, the sheath is said to be ion rich and an 'ion sheath'. On the other hand, if the sheath is electron rich, like for a Langmuir probe biased in the electron saturation region, it will be an 'electron sheath'.

The sheath theory is further divided into two regimes, depending on the ratio between the Debye length and the probe radius λ_D/r_p, where the Debye length, the characteristic shielding distance, is given by

$$\lambda_D = \sqrt{\frac{k_B \epsilon_0 T_e}{q_e^2 n_e}}. \tag{2.7}$$

For the case when the Debye length is much larger than the probe radius, $\lambda_D/r_p \gg 1$, the probe will be in the thick sheath regime, while when the Debye length is much smaller than the probe radius, $\lambda_D/r_p \ll 1$, the probe will be covered by the thin sheath regime.

2.1. *Presheath*

In between the sheath and the plasma there will be a presheath, where quasi-neutrality has been established, and electrons and ions are accelerated by the electric forces due to the potential drop (Chen 2016). In addition, pressure gradients can occur caused by the reduced density (Scheiner *et al.* 2015). To enter into the sheath, particles need to be accelerated beyond the Bohm velocity. In this study, we are simulating a collisionless plasma, and the drift of new particles into the presheath region is only caused by the thermal velocity of the particles. However, sheath disturbances generating an increase in the thermal velocity have been seen in the presheath. This will influence the ion distribution function, which will be distorted (Miloch *et al.* 2011; Gulbrandsen, Miloch & Fredriksen 2013).

3. Temporal effects for Langmuir probes

For a swept Langmuir probe, the applied bias will be a linearly ramped voltage, normally applied by a symmetrical sawtooth waveform. In this case, the frequency must be sufficiently low for the sheath to be established, and the particles must have time to traverse the sheath. This relates further to the ion speed, determined by the retarding probe potential and the ion mass. However, other limiting constraints are also present and a good overview of temporal effects for a Langmuir probe can be found in the study by Lobbia & Gallimore (2010) where five temporally constraining issues are discussed: 1 sheath formation time,

https://doi.org/10.1017/S0022377822001027 Published online by Cambridge University Press

2 sheath transit times, 3 plasma resonances, 4 polarisation drifts and 5 capacitive effects due to sheath capacitance, stray capacitance and mutual capacitance. In our study, we will focus on the formation time, and we will only briefly discuss other temporal limitations.

3.1. *Sheath formation time*

When the probe potential changes, or if the temperature or density of the plasma changes, the sheath changes its size and density composition. The simulated densities and temperatures represents an ionospheric plasma and will in our study respectively range from 1.0×10^9 to 1.0×10^{13} m^{-3} and 0.0181 to 18.1 eV. We are also throughout the text assuming a quasi-neutral stationary plasma where $T_e = T_i$. With the given parameters, the electrons will adapt within a few microseconds.

In this study, we distinguish between the formation time and the stabilisation time. The formation time is restricted to the time it takes to form the sheath by moving the ions out of the sheath and into the pre-sheath. After the formation time, there will be a period where oscillation and fluctuations can occur, which will eventually fade out. This will be referred to as stabilisation or relaxation time. Based on numerical studies of the sheath formation, it has been suggested that it takes between a few and ten ion plasma cycles before the sheath has been fully established (Nikiforov, Kim & Rim 2003)

$$\tau_{sheath} \approx 10 f_{ion}^{-1}, \tag{3.1}$$

where the plasma frequency f is given by $f = \omega_{pi}/2\pi$ and where ω_{pi} is given by the relationship between density n and the ion mass m

$$\omega_{pi} = \sqrt{\frac{n_i Z^2 e^2}{m_i \epsilon_0}}. \tag{3.2}$$

Most of the theory builds upon a study of the mapping of the sheath thickness and sheath edge based on solving Poisson's equations. The analytic expression for the time interval τ, which characterises the sheath's approach to the stationary state, was for a one-dimensional, uni-polar ion sheath derived by Kos & Tskhakaya (2018) to be

$$\tau = \frac{1}{\omega_{pi}\lambda}, \tag{3.3}$$

where λ is the characteristic rate for approaching the stationary state, described by the Child–Langmuir law.

Another approach to determine the sheath formation time is by the approximation is presented by (Lobbia & Gallimore 2010)

$$\tau_{sheath} \approx \frac{4 V_{sheath}}{A_{sheath} v_{ion}}, \tag{3.4}$$

where V_{sheath} is the sheath volume, A_{sheath} is the sheath area and v_{ion} is the ion flow speed.

For a spherical probe, this can further be expressed by the Debye length, electron temperature, ion mass and the probe radius r_p

$$\tau_{sheath} \approx 2(r_p + \lambda_D)/\sqrt{k_B T_e/m_i}. \tag{3.5}$$

https://doi.org/10.1017/S0022377822001027 Published online by Cambridge University Press

3.2. *Sheath traverse time*

The sheath traverse time describes the time it takes for a particle to move from the edge into the surface of the probe. In our study, where we consider a positively biased probe in the electron saturation region and no negatively charged ions, it will be the time it takes for the electrons to reach the probe. Since the electrons move about $\sqrt{m_i/m_e}$ faster than the ions, the formation time will exceed the traverse time and in our case not be observable. However, if negative ions are present and the probe is operated in swept bias mode, the ion current can be underestimated as the negative ions will not have sufficient time to reach the probe.

3.3. *Capacitive sources*

In a Langmuir system, several capacitive sources will exist. For all probes immersed in plasma, a capacitance between the probe and plasma sheath will be present. Other sources like stray capacitance between the probe line and the ground level and a mutual capacitance between neighbouring conductors can occur (Kjølerbakken, Miloch & Røed 2021). Contamination of the probe itself can also be related to capacitive effects on Langmuir probes (Brace 1998).

3.3.1. *Sheath capacitance*

The sheath, which shields out the probe potential and couples the probe to the plasma, acts like a component with capacitive properties in parallel with the sheath resistance. The probe sheath capacitance C_{sheath} is, in general, given by (Crawford & Grard 1966)

$$C_{sheath} = \alpha \frac{\epsilon_0 A_{probe}}{\lambda_d}, \tag{3.6}$$

where α is in the range 0.1 to 1.0 and is determined based on experimental data. For a spherical probe with the probe radius r_p and where $\lambda_d \gg r_p$ this can further be expressed as

$$C_{sheath} = \frac{4\pi\epsilon_0 r_p^2}{\lambda_d}. \tag{3.7}$$

The capacitance for our probe with a radius of 10 mm and a Debye length ranging from 1 to 100 mm will be in the range from 1 to 12 pF.

Capacitive effects are well known and capacitive probes are for used for radio frequency probes like sweeping impedance probes and high frequency capacitance probes (Barjatya & Swenson 2006; Muralikrishna, Vieira & Abdu 2007; Spencer & Patra 2015). It has also been shown that the capacitive effect is small for low frequencies (Kjolerbakken *et al.* 2022). We can assume that the time constant τ given by the product of the resistance R and capacitance C, $\tau = RC$ will be small for systems presented in this paper, since the resistance caused by the shield will be small as the sheath needs time to form.

4. Probe currents

The current collected by a Langmuir probe can be divided into three main categories: (i) the current of particles collected due to the thermal energy of the particles, where moving particles are colliding with the probe; (ii) current caused by particles attracted to the probe in an electric field; (iii) capacitive current that will occur when there is a change in the voltage potential applied to the probe, either by a step or by an alternating signal. The collected current of attracted particles can be approximated depending on the thickness of the shield by either: the sheath limit current, used when the sheath size is small compared

https://doi.org/10.1017/S0022377822001027 Published online by Cambridge University Press

with the size of the probe, or orbit motion limited (OML) current used when the sheath size is much larger than the size of the probe. In this study, the probe relation λ_d/r_p will be from 0.5 to 10 and go from the thin sheath regime to the thick sheath regime.

When a particle's kinetic energy is too small to escape from the electric field caused by the probe potential, it will be collected by the probe. This current is referred to as the sheath limited current. The thin sheath limited current is in general form given by

$$I_s^{thin} = 4\pi r_e^2 q_s n_0 \int_0^\infty v^3 f_s(\boldsymbol{v})\,\mathrm{d}v, \quad r_p > r_e, \tag{4.1}$$

where r_p is the probe radius, r_e is the radius of the sheath edge, $\boldsymbol{v}$ is the velocity vector, v is the particle velocity $v = \| \boldsymbol{v} \|$, n_0 is the ambient density of the species s and f_s is the normalised velocity distribution function of the species. For a spherical probe given an isotropic Maxwellian velocity distribution

$$f_s = A \exp\left[-\frac{v^2}{2v_{th}^2}\right], \tag{4.2}$$

where $v_{th,s} = \sqrt{k_B T_s/m_s}$, and the normalisation,

$$A = \frac{1}{(2\pi v_{th,s})^{3/2}}, \tag{4.3}$$

the thin sheath electron saturation for currents will be given by

$$I_e^{sat} = \pi r_p^2 n_e e v_e, \quad r_p > \lambda_D, \tag{4.4}$$

for the electron velocity v_e.

In the thick sheath regime where $\lambda_d/r_p \gg 1$, and given a spherical or cylindrical probe, the particles may follow a hyperbolic trajectory in orbits around the probe and in general form the saturation current is given by the OML theory as

$$I_s^{thick} = 4\pi r_e^2 q_s n_0 \int_0^\infty v^3 f_s(\boldsymbol{v}) \left(1 + \frac{|q_s \Phi_p,|}{\frac{1}{2} m v_s^2}\right) \mathrm{d}v, \quad r_p \ll r_e, \tag{4.5}$$

where Φ_p represents the potential of the probe. For a spherical probe and a Maxwellian velocity distribution, the electron saturation current is given by (Pilling & Carnegie 2007)

$$I_s^{OML} = I_e^{sat}\left(1 + \frac{e\Phi_p}{kT_e}\right)^\beta, \quad r_p < \lambda_D. \tag{4.6}$$

For a spherical probe, β equals to 1. However, this is only valid for a collisionless, non-drifting, Maxwellian distributed and non-magnetised plasma and in practice β should be fitted empirically (Barjatya & Merritt 2018; Marholm & Marchand 2020).

5. Numerical set-up

In our study, the PTetra model was used. PTetra is a full kinetic particle-in-cell (PIC) model following a standard PIC scheme on an unstructured grid (Marchand 2012; Marchand & Lira 2017). The particles are initiated with Boltzmann distributed velocity and move within the defined volume by integrating the Lorentz force with a second-order

https://doi.org/10.1017/S0022377822001027 Published online by Cambridge University Press

Debye length/probe radius	0.1	0.5	1.0	2.0	3.0	4.0	5.0	10
Debye length, (m)	0.001	0.005	0.01	0.02	0.03	0.04	0.05	0.1
Temperature (eV), fixed density $n = 1 \times 10^{11}$ m^{-3}	0.00181	0.04525	0.181	0.724	1.63	2.90	4.53	18.10
Density m^{-3}, fixed temperature $T = 0.181$ eV	1.0×10^{13}	4.0×10^{13}	1.0×10^{11}	2.5×10^{10}	1.1×10^{10}	6.2×10^{9}	4.0×10^{9}	1.0×10^{9}

TABLE 1. Simulation parameters for different spherical probe sizes.

accuracy leapfrog scheme. To avoid instabilities and artificial heating, it is required that the length traversed for each time step Δx is resolved within the Debye length: $\Delta x < \lambda_D$ (Birdsall & Maron 1980; Birdsall 1985). The PTetra model computes the time step based on the change in speed and acceleration, so no particles traverse more than the length of one grid cell within a single time step. The geometry and mesh were generated by Gmsh, which is an open-source meshing tool (Geuzaine & Remacle 2009). The spatial scale of the probe must be resolved within the grid (Okuda 1972). However, since the PTetra model uses an unstructured grid, objects only need to be resolved locally. The probe was a spherical probe with a radius of 1 cm inside a computational volume limited by an outer sphere with a radius ranging from 40 to 60 cm. The inner mesh resolution was set to 2 mm and the outer mesh resolution was 40 mm. Simulation parameters for the generated mesh are listed in table 1.

The initial condition of the plasma was a quasi-neutral plasma with Boltzmann distributed velocities, given by the initiated ion and electron temperature. All the plasma is taken to be collisionless, also in the sheath regions, and we are assuming non-drifting plasma with no external magnetic fields. For all simulations, the ions were H^+ ions, except for when heavier ions were studied and masses from 1, 2, 4, 8 to 16 atomic mass unit (amu) were compared.

In the study, three probe biases, 3, 5 and 7 V, were compared for different Debye lengths. The Debye length can be changed by changing either the temperature or the density of the plasma. First, we simulated the different Debye lengths by changing the temperature and the particle density was fixed. For the 5 V case, we also simulated the same Debye lengths by having a fixed temperature at 0.181 eV and instead changed the particle density from 1.0×10^9 to 1.0×10^{13} m^{-3}. The raw data were rather noisy and was filtered using an exponential moving average filter where, the relaxation time of $\tau = 0.2\,\mu$s was selected to be sufficiently small to not affect the transformation time.

6. Numerical results

The development of ion and electron densities and the current, as seen in figure 1, was studied over a period of 100 μs with an emphasis on the first 20 μs, where the sheath formation takes place. Figure 2(*a*) shows the probe current over the first 20 μs and the time stamp for when the spatial density result, seen in figure 2(*b*,*c*), was extracted. As seen in figure 2 the temporal effects have been categorised into two periods: the formation period and the relaxation period. In the formation period the distribution of ions and electrons takes place and it is limited by the time it takes for the ions to move out of the sheath region. The probe current will also reach the expected level during this period. However,

https://doi.org/10.1017/S0022377822001027 Published online by Cambridge University Press

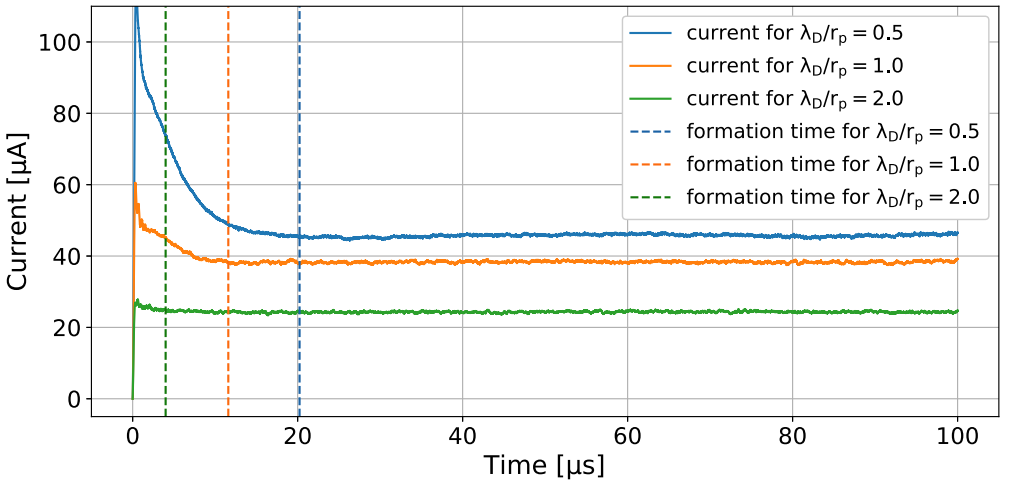

FIGURE 1. Sheath formation time for $\lambda_D/r_p = 0.5$, 1 and 2 with T_e respectively 0.04525, 0.181 and 18.1 eV. The bias was 5 V and the $n_e = n_i = 1.0 \times 10^{11}$ m^{-3}. The formation time is taken to be the point where the current has reached a stable level.

fluctuations and oscillations may occur, and the period from when the formation is done to when a stable current (steady state) is established will be referred to as the relaxation period. The collected current at 100 μs was also compared with the OML theory, as seen in figure 3, with a good agreement for simulations where the Debye length exceeds the dimensions of the probe. The sheath formation time was derived from the current at the point where the derivative of the current was equal to zero and the current was within 2 per cent of the average current in the subsequent 2 μs. This algorithm seemed to agree well with results from the analysis of the particle distribution that we can see in figure 2. Examples of sheath formation times can be seen in figure 1 for $\lambda_D/r_p = 0.5$, 1 and 5.

6.1. *Temperature dependency*

The sheath formation time for plasma temperatures from ranging from 0.0181 to 18.1 eV was simulated for probe biases at 3, 5 and 7 V where the plasma density was fixed at 1×10^{11} m^{-3}. In figure 4, the extracted sheath formation times are shown as a function of the temperature and the relationship between the corresponding Debye length and the probe radius λ_D/r_p. For Debye lengths greater than the probe radius, the bias does not have a significant influence on the sheath formation time and for temperatures giving a λ_D/r_p relationship larger than 4 the formation time seems to be less affected by the temperature as well.

In figure 5 we see the particle distribution for Debye length/probe radius from 0.5 to 10 given by temperatures from 0.04525 to 18.1 eV. When the probe is operated in the thin sheath regime, it has a thicker sheath than when it is operated in the thick sheath regime. This can be miss leading. However, we must keep in mind that the Debye length for the $\lambda_D/r_p = 0.5$ is 5 mm and the Debye length for the $\lambda_D/r_p = 10$ is 100 mm and the sheath size is relative to the Debye length and not the probe radius. In addition, the density variations for the thick sheath are small, and it is difficult to determine the actual sheath size based on these results.

https://doi.org/10.1017/S0022377822001027 Published online by Cambridge University Press

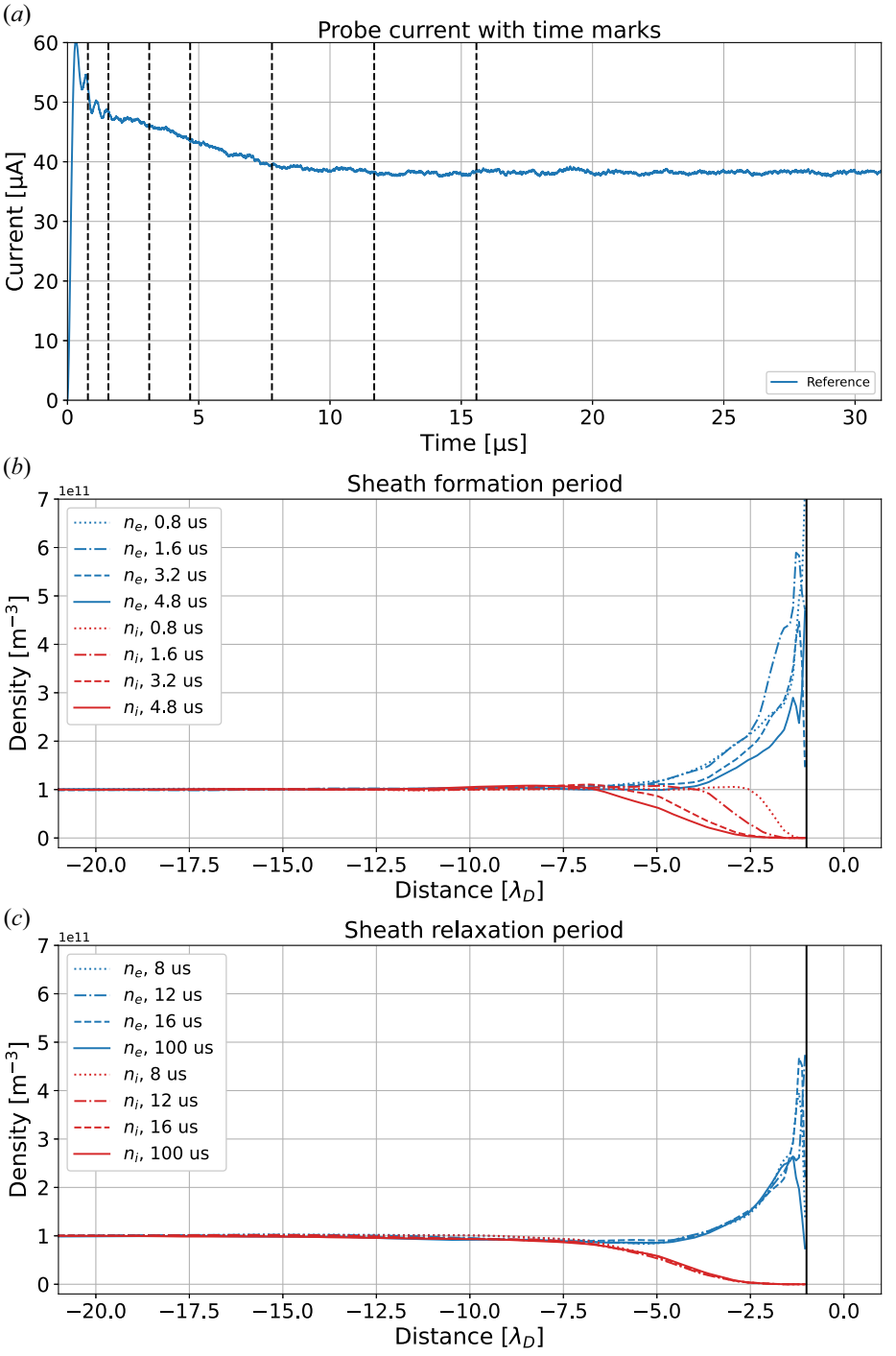

FIGURE 2. Ion and electron density as a function of the radius normalised to the Debye length. The data are the mean value densities at a given radial distance from the probe along the x, y and z axes in both positive and negative directions. The density is plotted for each of the time stamps shown in the upper figure and categorised respectively into the formation period or the relaxation period. Here, $\lambda_D/r_p = 1$, $T_e = 0.181$ eV, the probe bias was 5 V and the density of the ambient plasma was $n_e = n_i = 1.0 \times 10^{11}$ m^{-3}.

https://doi.org/10.1017/S0022377822001027 Published online by Cambridge University Press

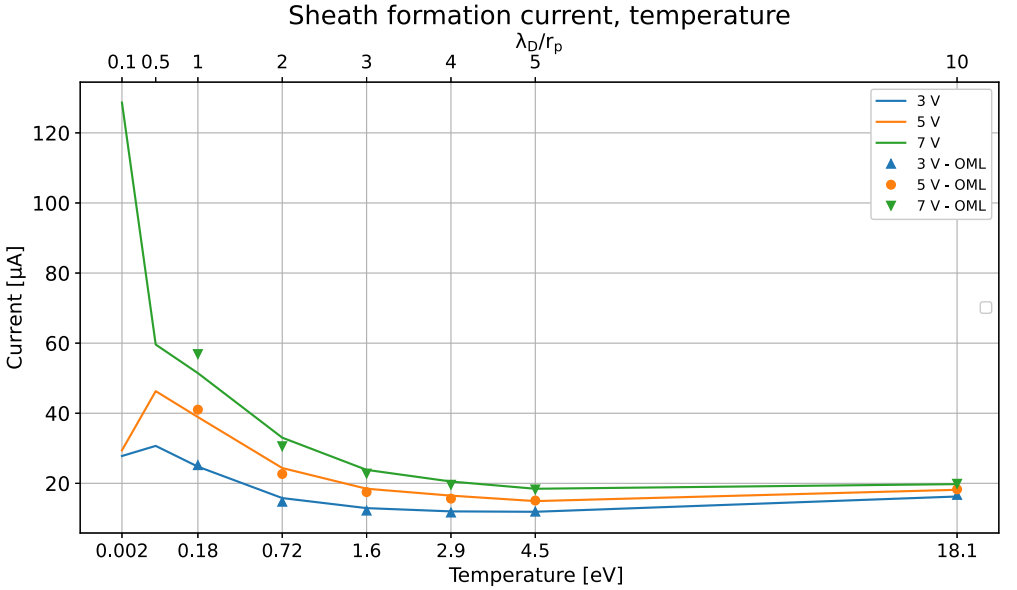

FIGURE 3. Simulated currents for probe biases at 3, 5 and 7 V for temperatures from 0.0181 to 18.1 eV compared with the currents given by the OML theory. The plasma density was fixed at 1×10^{11} m^{-3}.

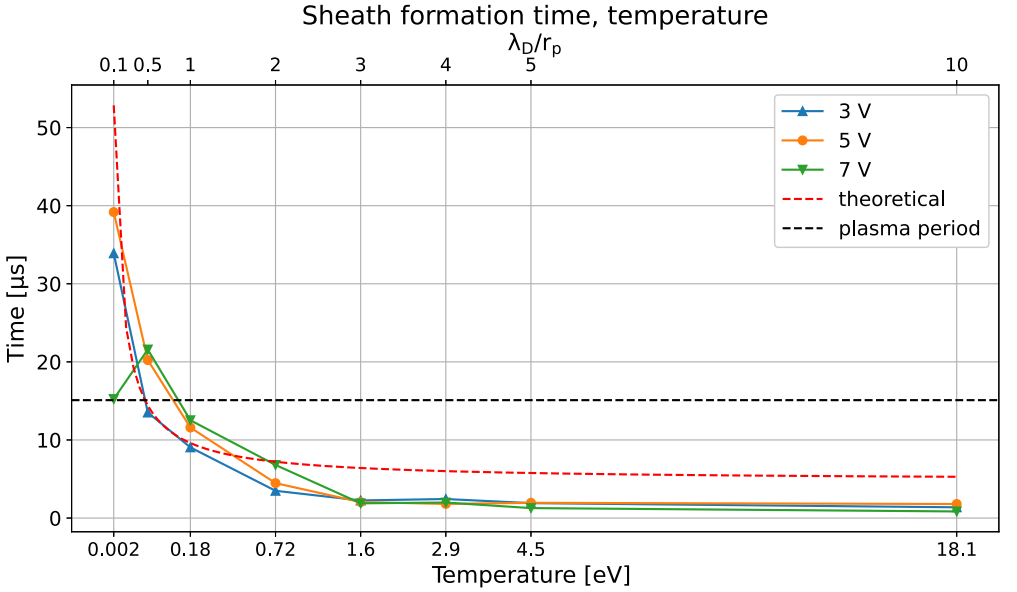

FIGURE 4. Sheath formation times for plasma temperatures from 0.0181 to 18.1 eV and plasma density fixed at 1×10^{11} m^{-3}. The probe was biased at 3, 5 and 7 V.

We also observe that the sheath goes from a classic monotonic sheath in the thin sheath regime to a non-monotonic in the thick sheath regime where a potential well forms and a fraction of the repelled electrons are returned to the probe (Hobbs & Wesson 1967; Wang *et al.* 2016)

https://doi.org/10.1017/S0022377822001027 Published online by Cambridge University Press

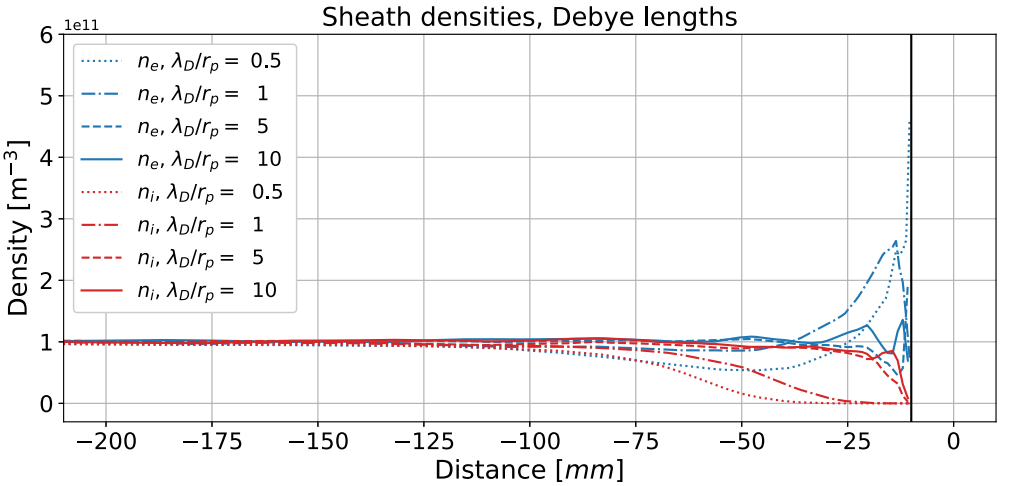

FIGURE 5. Particle distribution for Debye length/probe radius from 0.5 to 10 given by temperatures from 0.04525 to 18.1 eV. The plasma density was fixed at 1×10^{11} m^{-3} and the probe was biased at 5 V.

6.2. *Density dependency*

Figure 6 shows the formation time for a probe biased at 5 V with densities ranging from 1.0×10^{9} to 1.0×10^{13} m^{-3}, and the temperature fixed at 0.181 eV compared with the same temperature simulations presented in figure 4 at 5 V with temperatures ranging from 0.0181 to 18.1 eV and the density fixed at 1×10^{11} m^{-3}. Both simulations give the same Debye length vs. probe radius relationship. The theoretical corresponding values, given by (3.5), were compared. We see that using a Debye length as a guiding measure for the formation time is misleading. However, in the thin sheath it makes sense to relate it to the plasma frequency, which is a density dependent quantity, as expressed in (3.1). In figure 7 we see that the sheath size is comparable for the two cases, where the upper curves have a plasma temperature of 18.1 eV and a density of 1.0×10^{11} m^{-3} and the lower curves have a plasma temperature of 0.181 eV and a density of 1.0×10^{13} m^{-3}, both curves having the same Debye lengths.

6.3. *Mass dependency*

Figure 8 shows the formation time as a function of the ion mass, ranging from 1 to 16 amu. The probe was biased at 3, 5 and 7 V, the temperature was 0.181 eV and the density was 1×10^{11} m^{-3} giving a Debye length equal to the probe radius. For all probe biases, we find that the simulated result agrees well with Lobbia's approximation, where a quadrupling of the ion mass approximately doubles the time.

Since the sheath edge is depends on the energy and the energy distribution of the particles, we expect the same distribution of particles, given the same energy and charge of the ions. This is confirmed by figure 9, showing a comparable distribution of ions and electrons in the sheath for hydrogen (1 amu) and oxygen (16 amu) ions. As expected, and according to OML theory and the thin sheath theory, the current is comparable for all ion masses, and we only see small variations at the same order as the noise. From figure 8 we also notice that the formation time is not noticeably affected by the probe bias and that all three probe potentials have comparable formation times.

https://doi.org/10.1017/S0022377822001027 Published online by Cambridge University Press

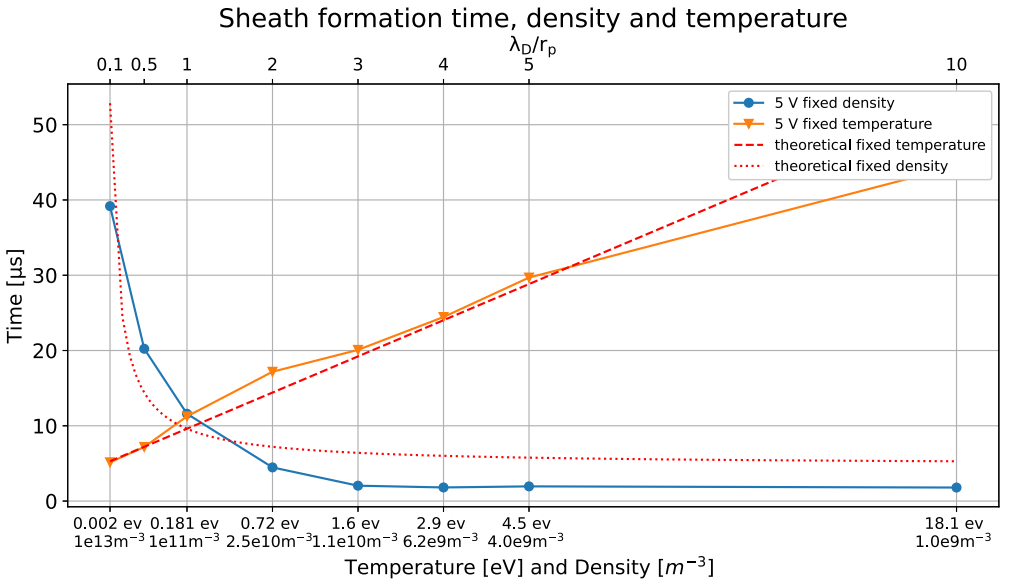

FIGURE 6. Comparison of sheath formation times for the same Debye lengths. The exponential line has varying temperature ranging from 0.00181 to 18.1 eV and a fixed density at 1.0×10^{11} m^{-3}. The linear curve has a varying density from 1.0×10^{9} m^{-3} to 1.0×10^{13} and fixed the temperature at 0.181 eV. The probe was for all cases biased at 5 V.

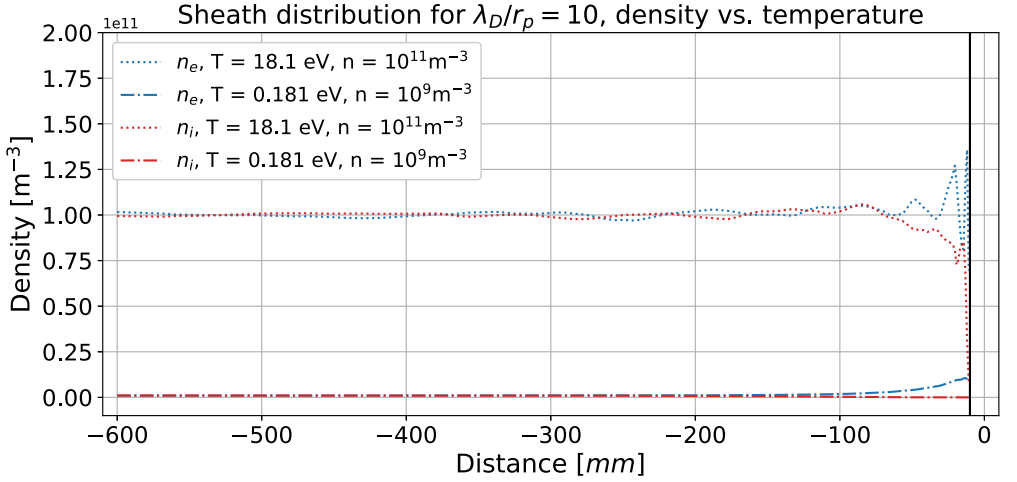

FIGURE 7. Sheath densities, the same Debye length, where the upper line has a plasma temperature of 18.1 eV and a density of 1.0×10^{11} m^{-3}, while the lower line has a plasma temperature of 0.181 eV and a density of 1.0×10^{13} m^{-3}. The probe was for all cases biased at 5 V.

7. Discussion and conclusion

The objective of this study was to better understand the formation times for a sheath in the vicinity of a spherical Langmuir probe, given a plasma that reflects the plasma we find in the ionosphere. We also wanted to see if theoretical frameworks correspond to simulated results. All our results compare well with the theoretical approximation for a

https://doi.org/10.1017/S0022377822001027 Published online by Cambridge University Press

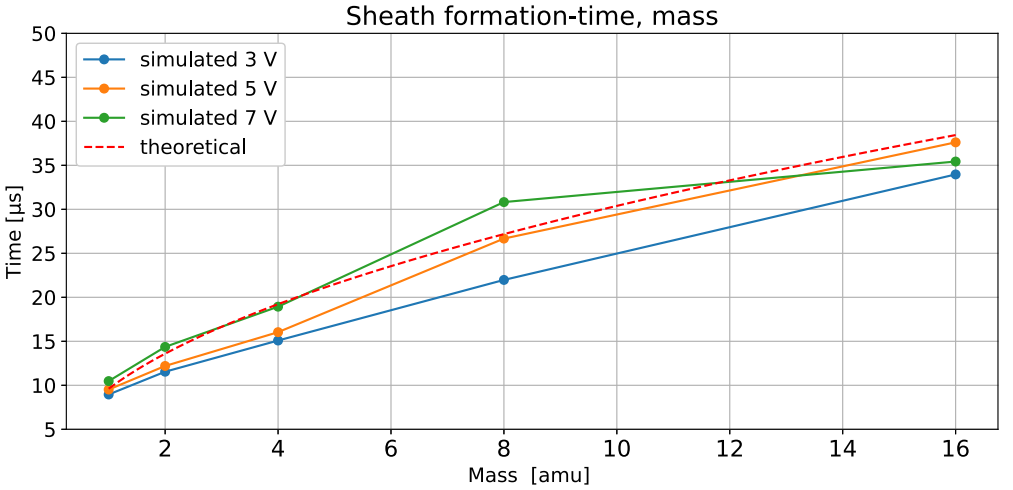

FIGURE 8. Sheath formation time for ion masses ranging from 1 to 16 amu. The probe was biased at 3, 5 and 7 V, the temperature was 0.181 eV and the density was 1×10^{11} m^{-3}.

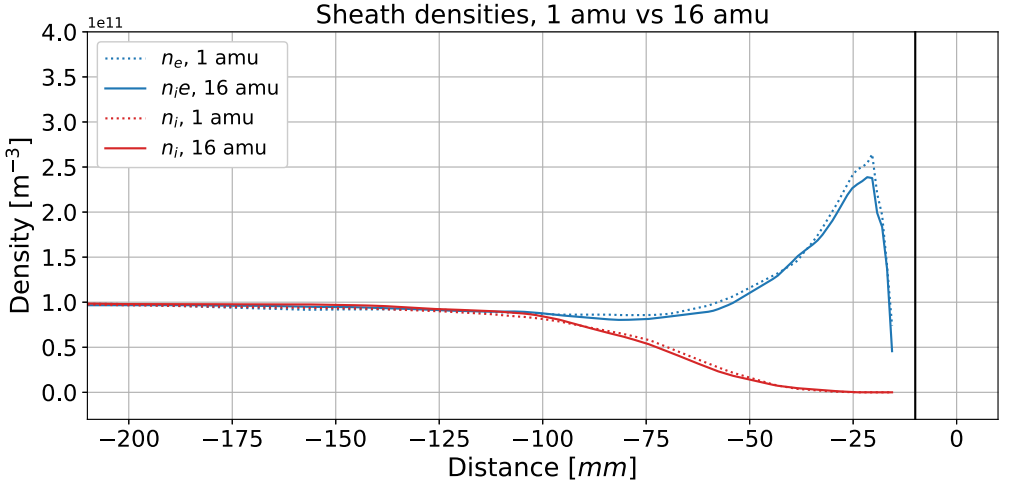

FIGURE 9. Sheath densities compared for ion masses 1 and 16 amu. The probe was biased at 3, 5 and 7 V, the temperature was 0.181 eV and the plasma density was fixed at 1×10^{11} m^{-3}.

spherical probe given by Lobbia in (3.5). This applies to both the thin and the thick sheath regime.

The applied bias voltage does not seem to be crucial to the formation time for probes in the thick sheath regime. However, for probes in the thin sheath regime, we see a stronger influence of the applied bias voltage, resulting in a slightly longer formation time. Our results, presented in figure 5, also show that, as we move into the thick sheath regime, the formation time is less affected by the plasma temperature and is dominated by the density of the plasma. In general, our results show that it is very useful to distinguish between the thick and thin sheath regimes.

https://doi.org/10.1017/S0022377822001027 Published online by Cambridge University Press

While several studies often relate both formation time and the sheath edge to the Debye length. Our results, as seen in figure 6, show that a given Debye length can have very different formation time and sheath size.

The simulated results for different ion masses, figure 8, show that a quadrupling of the ion mass approximately doubles the formation time. This demonstrates how an applied step function to the probe bias and the formation time given by Lobbia in (3.5), can be used to characterise ions species composition by their mass, assuming the temperature and density are known or to characterise the ion density when the ion species and mass are known.

For a swept bias system, the applied bias will be a linearly ramped voltage, and many small step functions. In this case, knowing the formation time allows sweeping frequencies to be configured and optimised for the actual plasma and allows higher sweeping frequencies to be used.

Acknowledgements

We would like to thank R. Marchand for making the PTetra model available for this study.

Editor Troy Carter thanks the referees for their advice in evaluating this article.

Declaration of interests

The authors report no conflict of interest.

Data Access Statement

The data that support our findings in this study are available from the corresponding author upon reasonable request.

Funding

This work is part of the 4DSpace Strategic Research Initiative at the University of Oslo. The work has been supported in part by the Research Council of Norway, grant number 275653a and the Sigma2 cluster, owned by the University of Oslo and Uninett/Sigma2, project number NN9761K.

REFERENCES

BARJATYA, A. & MERRITT, W. 2018 Error analysis of multi-needle Langmuir probe measurement technique. *Rev. Sci. Instrum.* **89** (4), 043507–043507.

BARJATYA, A. & SWENSON, C.M. 2006 Observations of triboelectric charging effects on Langmuir-type probes in dusty plasma. *J. Geophys. Res.* **111** (A10), A10302.

BASU, S., MACKENZIE, E. & BASU, S. 1988 Ionospheric constraints on vhf/uhf communications links during solar maximum and minimum periods. *Radio Sci.* **23** (3), 363–378.

BIRDSALL, C.K. 1985 Plasma physics via computer simulation. Taylor & Francis.

BIRDSALL, C.K. & MARON, N. 1980 Plasma self-heating and saturation due to numerical instabilities. *J. Comput. Phys.* **36** (1), 1–19.

BOYD, R.L.F. 1951 The mechanism of positive ion collection by a spherical probe in a dense gas. *Proc. Phys. Soc.* B **64** (9), 795–804.

BRACE, L.H. 1998 Langmuir probe measurements in the ionosphere.

CHEN, F. 2016 *Introduction to Plasma Physics and Controlled Fusion*, 3rd edn. Springer.

CRAWFORD, F.W. & GRARD, R. 1966 Low-frequency impedance characteristics of a Langmuir probe in a plasma. *J. Appl. Phys.* **37** (1), 180–183.

https://doi.org/10.1017/S0022377822001027 Published online by Cambridge University Press

FOLLESTAD, A.F., HERLINGSHAW, K., GHADJARI, H., KNUDSEN, D.J., MCWILLIAMS, K.A., MOEN, J.I., SPICHER, A., WU, J. & OKSAVIK, K. 2020 Dayside field-aligned current impacts on ionospheric irregularities. *Geophys. Res. Lett*. **47** (11).

GEUZAINE, C. & REMACLE, J.-F. 2009 Gmsh: A 3-d finite element mesh generator with built-in pre- and post-processing facilities. *Intl J. Numer. Meth. Engng* **79** (11), 1309–1331.

GULBRANDSEN, N., MILOCH, W.J. & FREDRIKSEN, Å. 2013 Interpretation of ion velocity distributions measured with a grounded retarding field energy analyzer (RFEA) in an inductively coupled helicon plasma. *Contrib. Plasma Phys*. **53** (1), 27–32.

HOBBS, G.D. & WESSON, J.A. 1967 Heat flow through a Langmuir sheath in the presence of electron emission. *Plasma Phys*. **9** (1), 85–87.

JIN, Y., MOEN, J.I. & MILOCH, W.J. 2014 GPS scintillation effects associated with polar cap patches and substorm auroral activity: direct comparison. Jin, Yaqi (2016) Characterization of GPS Scintillations in the Polar Ionosphere. Doctoral thesis. http://urn.nb.no/URN:NBN:no-55915.

KJOLERBAKKEN, K.M., MILOCH, W.J., MARTINSEN, O.G, PABST, O. & ROED, K. 2022 Numerical study of non-linear effects for a swept bias Langmuir probe. *IEEE Trans. Plasma Sci*. **50** (5), 1237–1245.

KJØLERBAKKEN, K.M., MILOCH, W.J. & RØED, K. 2021 The influence of probe spacing and probe bias in a double Langmuir probe setup. *AIP Adv*. **11** (8), 085007–085007–9.

KOS, L. & TSKHAKAYA, D.D. 2018 Theory of ion-matrix-sheath dynamics. *AIP Adv*. **8** (1), 015202.

LOBBIA, R. & GALLIMORE, A. 2010 Temporal limits of a rapidly swept Langmuir probe. *Phys. Plasmas* **17**, 073502.

MARCHAND, R. 2012 Ptetra, a tool to simulate low orbit satellite–plasma interaction. *IEEE Trans. Plasma Sci*. **40** (2), 217–229.

MARCHAND, R. & LIRA, P.A.R. 2017 Kinetic simulation of spacecraft–environment interaction. *IEEE Trans. Plasma Sci*. **45** (4), 535–554.

MARHOLM, S. & MARCHAND, R. 2020 Finite-length effects on cylindrical Langmuir probes. *Phys. Rev. Res*. **2** (2), 023016.

MILOCH, W.J., GULBRANDSEN, N., MISHRA, L.N. & FREDRIKSEN, Å. 2011 Ion velocity distributions in the sheath and presheath of a biased object in plasma. *Phys. Plasmas* **18** (8), 083502–083502–6.

MOEN, J., OKSAVIK, K., ALFONSI, L., DAABAKK, Y., ROMANO, V. & SPOGLI, L. 2013 Space weather challenges of the polar cap ionosphere. *J. Space Weather Spac*. **3**, A02.

MOTT-SMITH, H.M. & LANGMUIR, I. 1926 The theory of collectors in gaseous discharges. *Phys. Rev*. **28**, 727–763.

MURALIKRISHNA, P., VIEIRA, L.P. & ABDU, M.A. 2007 Spectral features of e- and f-region plasma irregularities as observed by rocket-borne electron density probes from Brazil. *Rev. Bras. Geofís*. **25** (Suppl 2), 115–128.

NIKIFOROV, S.A., KIM, G.-H. & RIM, G.-H. 2003 Dynamics of high-voltage pulsed cylindrical sheath. *IEEE Trans. Plasma Sci*. **31** (1), 94–103.

OKUDA, H. 1972 Nonphysical noises and instabilities in plasma simulation due to a spatial grid. *J. Comput. Phys*. **10** (3), 475–486.

PILLING, L.S. & CARNEGIE, D.A. 2007 Validating experimental and theoretical Langmuir probe analyses. *Plasma Sources Sci. Technol*. **16** (3), 570.

RIEMANN, K.U. 1991 The Bohm criterion and sheath formation. *J. Phys. Appl. Phys*. **24** (4), 493.

SCHEINER, B., BAALRUD, S.D., YEE, B.T., HOPKINS, M.M. & BARNAT, E.V. 2015 Theory of the electron sheath and presheath. *Phys. Plasmas* **22** (12), 123520.

SPENCER, E. & PATRA, S. 2015 Ionosphere plasma electron parameters from radio frequency sweeping impedance probe measurements. *Radio Sci*. **50** (9), 853–865.

WANG, X., PILEWSKIE, J., HSU, H.-W. & HORÁNYI, M. 2016 Plasma potential in the sheaths of electron-emitting surfaces in space. *Geophys. Res. Lett*. **43** (2), 525–531.